Chapter

Magnesium-Based Materials for Hydrogen Storage: Microstructural Properties

Ryota Kondo and Takeshita T. Hiroyuki

Abstract

Magnesium (Mg) is hydrogenated as core-shell-type hydride. Therefore, increase of absorption capacity to the theoretical hydrogen capacity is still one of the most important issues for the hydrogen storage materials. In this study, the procedure of the core-shell structure as well as effect of Al concentration in Mg on the growth MgH2 in Mg were investigated. MgH2 was formed on the surface as well as inside of unreacted Mg core. The inside MgH2 was formed in a granular form on Mg grain boundary and its size increased by applying plastic deformation. Thickness of the surface MgH2 and size of the internal MgH2 increased with an increase in hydrogenation time until the hydride surface was completely covered with MgH2. However, the growth of the surface and internal MgH2 came to a halt after the surface was covered with MgH2. From these results, supplying H from metal side was dominantly contributed for growth of the surface and internal MgH2 because diffusion rate of H in Mg was much higher than that in MgH2. In addition, the growth of internal MgH2 as well as control of surface MgH2 can contribute to the promotion of the complete hydrogenation of Mg-based hydrogen storage materials.

Keywords: magnesium, hydride, internal, three-dimension, surface, microstructure, distribution, grain boundary

1. Introduction

Magnesium (Mg) can store 7.6 mass% of hydrogen after formation of magnesium hydride (MgH_2), which has attractive features for hydrogen storage material such as low cost, abundant resource and light weight [1]. However, dehydrogenation temperature is very high (560 K at 0.1 MPaH_2) because MgH_2 is thermodynamically stable ($\Delta_r H$ = −72.8 ± 4.2 kJ mol^{-1}, $\Delta_r S$ = −142 ± 3 J K^{-1} mol^{-1}) [2]. In addition, their hydrogenation/dehydrogenation kinetics is also lower, then the conditions of hydrogenation and dehydrogenation are severe and core-shell-type hydride is formed. In order to obtain MgH_2 completely from Mg and effectiveness of hydrogenation/dehydrogenation process, it is necessary to finely pulverize, severe plastic deformation, heat treatment for a long time, and addition of catalyst [3–10].

Mg is a metal and when it reacts with H_2, MgH_2 forms an ionic bond and a weak covalent bond between Mg-H and the valence number of the ion is indicated as $Mg^{1.91+}$ and $H^{0.26-}$ [11]. The diffusion coefficient of H in MgH_2 is several order of magnitude lower when compared to that in Mg: D_H^{Mg} = 7 × 10^{-11} m^2 s^{-1}

(300 K) in Mg and $D_H^{MgH2} = 1.1 \times 10^{-20}$ m^2 s^{-1} (305 K) in MgH_2 [12, 13]. Based on these characteristics, powder Mg forms core-shell-type structure hydride, MgH_2 as a shell and unreacted Mg remains in the core [14, 15] making progress of completely hydrogenation difficult. On the other hand, the hydrogen partial pressure has a great influence on the progress of the hydrogenation. When the hydrogen partial pressure is high, since MgH_2 quickly covers the Mg powder surface, hydrogenation halts and the amount of hydride concentration decreases markedly, whereas when the hydrogen partial pressure is low, the time until MgH_2 covers the Mg surface extends, then the hydride concentration increases [16]. Therefore, to accomplish the efficient hydrogenation, the process of hydrogenation should be revealed.

As a result of investigation aiming at efficient hydrogenation, some curious microstructural characteristics were obtained, that is shell of MgH_2 and core Mg in addition to MgH_2 in the core Mg. In the following, MgH_2 on the surface layer named as MgH_2(sur) and that in Mg core named as MgH_2(int). MgH_2(int) formed in the Mg core is distinguished from MgH_2(sur). The particle size of MgH_2(int) in Mg^{-6} mass%, Al-1 mass%, Zn alloy was larger than that in pure Mg. This result shows the grain size of MgH_2(int) would be in correlation with Al concentration. Therefore, in this study, the influence of Al concentration in Mg on formation of MgH_2(int) is clarified. To reveal the mechanism of MgH_2(int) formation, coarse-type Mg-based hydrogen storage materials will be developed. Bulky hydrogen storage materials are attractive for handling, safety, and applying large module.

2. Materials and methods

Pure Mg manufactured by Rare Metallic Co., Ltd. and Mg- (3, 6, 9) mass%, Al-1 mass%, Zn alloy (hereinafter referred to as AZ31, AZ61, AZ91) manufactured by Sankyo Aluminum Co., Ltd. were used as samples. **Table 1** shows the composition of the samples.

As pretreatment, these samples were cut into prismatic shapes (8 mm in width, 5 mm in length, 3 mm in thickness) and then annealed, evacuated to 2×10^{-4} Pa in a stainless steel container, and replacing it with Ar gas (nominal purity 99.9999 vol%) was repeated several times and then heated under an Ar atmosphere of 3 kPa at a temperature of 723 K and a treatment time for 32.4 ks. For AZ61, annealed material (annealed) and 10% cold-rolled sample (cold-rolled) were subjected to hydrogenation (129.6 ks), respectively. An observation of the cross-sectional structure was carried out using an optical microscope (OM). Mg alloys are known to produce MgH_2 at low temperature by applying severe plastic deformation [17]. **Table 2** shows the crystal grain sizes of annealed Mg and AZ31, AZ61, and AZ91 alloys.

Material	Composition (mass%)							
	Al	Zn	Mn	Si	Fe	Cu	Ni	Ca
Mg	0.0013	0.0024	0.012	0.022	0.0016	0.0031	0.0003	0.01
AZ31	2.80	0.80	0.32	0.022	0.003	0.003	<0.002	
AZ61	6.26	0.63	0.26	0.015	0.005	0.001	0.0007	
AZ91	8.70	0.82	0.22	0.007	0.005	<0.002	0.002	

Table 1.
Composition of Mg and AZ31, AZ61, AZ91 alloys.

Material	Grain size, d/μm (standard deviation)
Mg	250 (70)
AZ31	34 (3.4)
AZ61	36 (4.8)
AZ91	40 (3.5)

Table 2.
Grain size of annealed Mg and AZ31, AZ61, and AZ91 alloys.

For hydrogenation of Mg alloys, these samples after annealing was dry-polished with SiC abrasive paper (# 320) in Ar gas circulation-type glove box (dew point −55 to −70°C, oxygen concentration 1 ppm or less), dry polished and immediately sealed in a stainless steel reaction vessel with a gasket made of stainless steel with Ag plating. In this reaction vessel, a sheath-type thermocouple was installed inside the container and the temperature in the vicinity of the samples was set. In order to generate MgH_2, hydrogenation was carried out at a hydrogen pressure of 3.61 MPa and a temperature of 673 K using a Siebert's type apparatus, and the nominal purity of the hydrogen gas used was 99.99999 vol%. The time was maintained in the range of 0–259.2 ks, and it is shown in parentheses here after.

The X-ray diffraction (XRD) instrument was used for the identification of MgH_2(sur). X-ray source of CuKα with the tube voltage of 40 kV and the tube current of 15 mA was used. Microstructure of MgH_2 was judged with presence or absence of charge up by using of scanning electron microscope (SEM). Crystal structure of MgH_2(int) was investigated using an electron beam backscatter diffraction (EBSD) analyzer.

Samples for microstructural observation and analysis were cut at a position of 4 mm which is half in the width direction and roughly polished using SiC polishing paper (# 320 → # 800 → # 1000) followed by an Al_2O_3 suspension (0.05 μm) or SiO_2 suspension (0.04 μm). Dehydrated methanol was used as the extension liquid. The sample after polishing was promptly washed with an ultrasonic washing machine in dehydrated methanol. After washing, the sample was dried using pure nitrogen gas (99.99%).

Three-dimensional analysis of MgH_2(sur) and MgH_2(int) was carried out based on data constructed by a continuous serial sectional method, and an optical microscope (OM) was used for microstructural observation. Information at the position and observation depth was obtained by driving a pyramidal indentation into the sample using a Vickers hardness instrument. ImageJ was used for geometrical analysis and the construction of the three-dimension image [18, 19].

Figure 1 described quantitative analysis method for obtaining information on the thickness of the MgH_2(sur) layer. In the analysis, five or more images are selected and the MgH_2 was observed as a dark area. The mean thickness (d_{av}) of MgH_2(sur) was calculated by dividing the area of each observed MgH_2(sur) by the length of MgH_2(sur) on the surface. Next, the shape of the surface is extracted. The surface line was translated in the direction of the inside. The maximum thickness of MgH_2(sur) was evaluated as the translated length at point of the surface line parted from MgH_2(sur) particle. The minimum thickness (d_{min}) was evaluated at the first point of intersection between the shape line and Mg. The average particle size of MgH_2(int) is calculated by calculating the area of MgH_2(int), and the value of the diameter calculated when assuming MgH_2(int) as a spherical calculation on average.

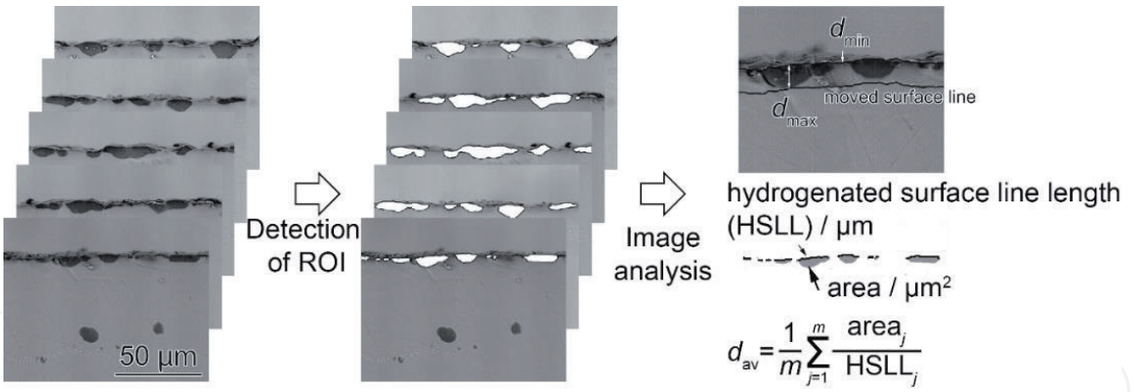

Figure 1.
Method of quantitative analysis for average (d_{av}), maximum (d_{max}) and minimum (d_{min}) thickness values of MgH_2(sur) from SEM-BSE images.

3. Results

Figure 2 shows the XRD pattern of hydrogenated Mg, AZ31, AZ61, AZ91 alloys for 1.8 ks. In all the samples, formation of MgH_2 was observed. These samples were not polished, therefore the information from XRD was mainly from MgH_2(sur). The peaks from Mg were shifted to higher angle side with Al concentration due to substitutional solid solution formation. On the other hand, in the peak pattern of MgH_2, obvious peak shifts were not observed with increase of Al concentration.

Figure 3 shows cross-sectional OM images of annealed and cold rolled AZ61 alloy. The annealed and cold rolled AZ61 exhibited both MgH_2(sur) (white arrow) and MgH_2(int) (black arrow). There were no difference on MgH_2(sur) between annealed and cold rolled AZ61 alloy as d_{av} was 9 μm (d_{max}: 22 μm, d_{min}: 2 μm) in annealed and d_{av} was 8 μm (d_{max}: 22 μm, d_{min}: 2 μm) in cold rolled condition. However, particle size of MgH_2(int) was lager in cold rolled condition than in

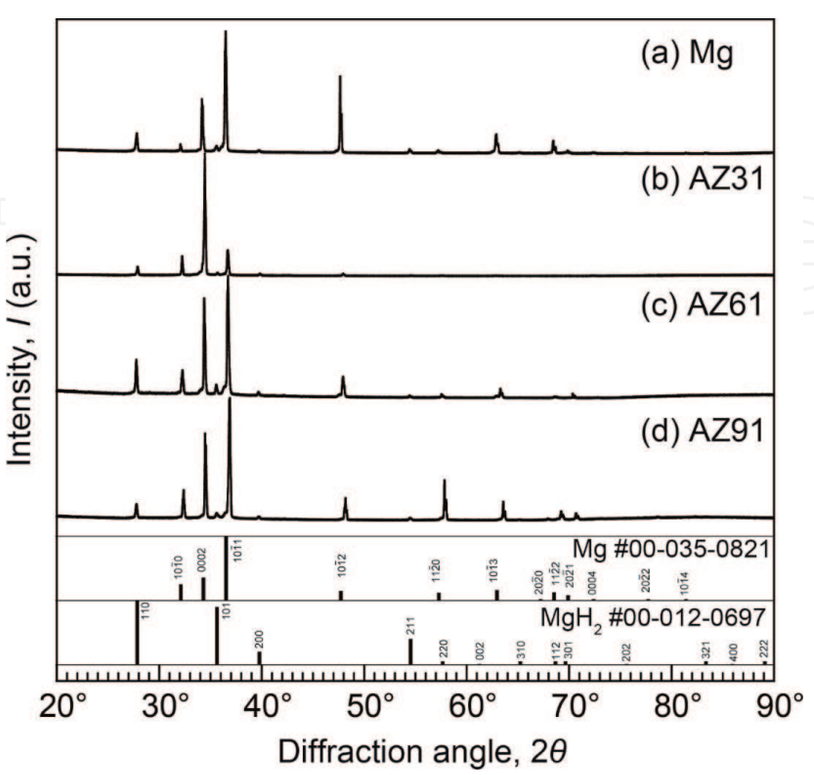

Figure 2.
XRD profiles of hydrogenated Mg, AZ31, AZ61 and AZ91 alloys at 673 K in 3.61 MPa H_2 for 1.8 ks.

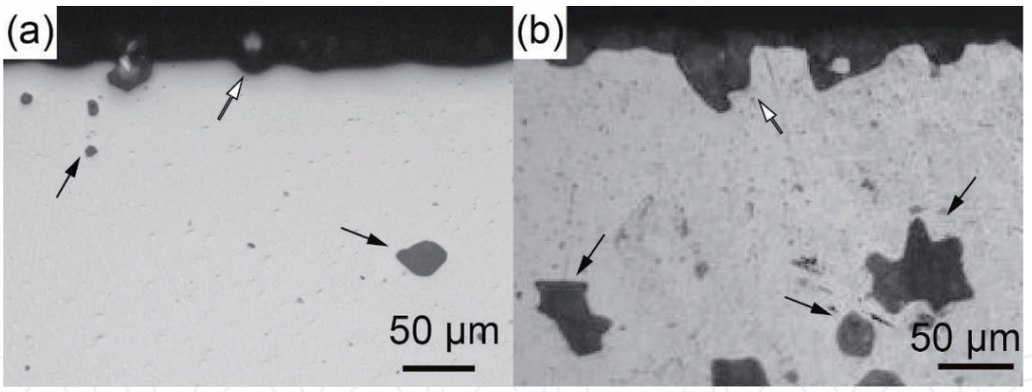

Figure 3.
Cross-sectional optical micrographs of hydrogenated AZ61 in 3.61 MPa H_2 at 673 K for 129.6 ks (a) annealed and (b) cold-rolled samples. Open and solid arrows point out MgH_2(sur) and MgH_2(int), respectively.

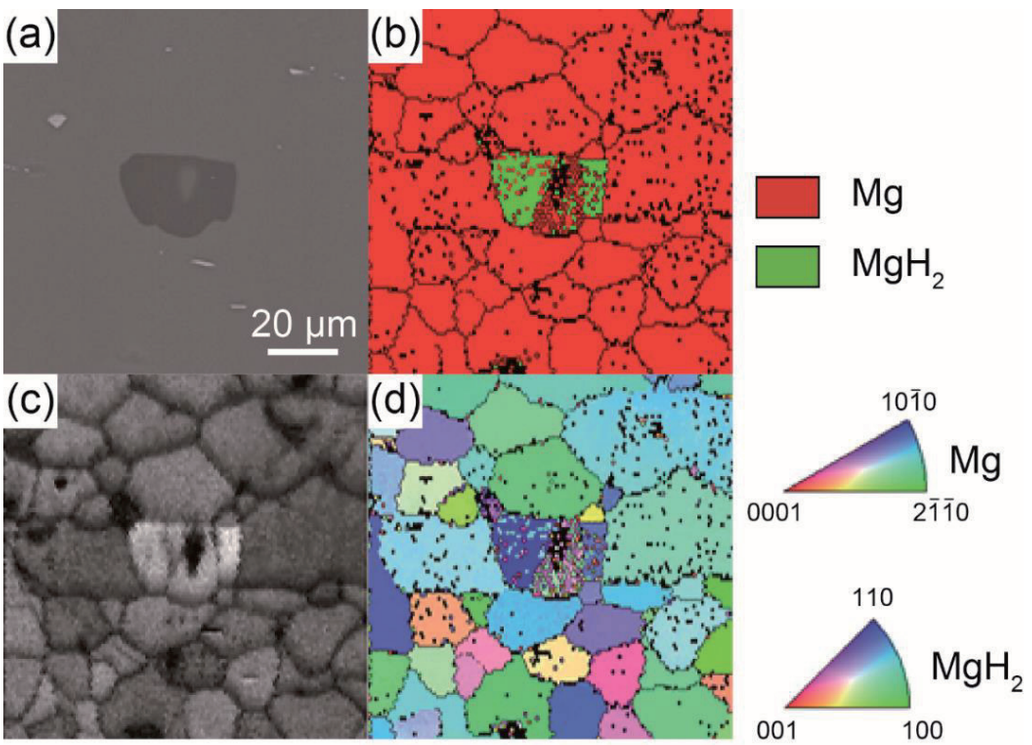

Figure 4.
SEM-EBSD analyzed images of AZ31 hydrogenated at 673 K in 3.61 MPa H_2 for 64.8 ks. (a) SEM-BSE image, (b) phase map, (c) IQ map, and (d) IPF.

annealed condition as mean diameter was 15 μm (maximum: 38 μm, minimum: 3 μm) in annealed condition and mean diameter was 53 μm (maximum: 125 μm, minimum: 14 μm) in cold rolled condition.

Figure 4 shows the SEM image and results of EBSD analysis of hydrogenated AZ31. **Figure 4** (a) shows the backscattered electron image (BSE), (b) shows the phase map in the same area with (a), (c) is image quality (IQ) map, and (d) is an inverse pole figure (IPF). In phase map (b), Mg was shown in red and MgH_2 was shown in green color. Comparing (a) and (b), dark area in BSE (a) corresponds to MgH_2 area in phase map (b). As focused on IQ map (c), image quality of MgH_2 area was lower than that of Mg area. The decrease of quality at MgH_2 was due to high volume change between Mg to MgH_2 about 32% as the result of residual strain and/or nonconducting material; MgH_2 tends to charge up.

The MgH_2(int) observed in **Figures 3** and **4** was surrounded with metallic Mg, and the MgH_2(int) has not interface with hydrogen gas at glance. Therefore,

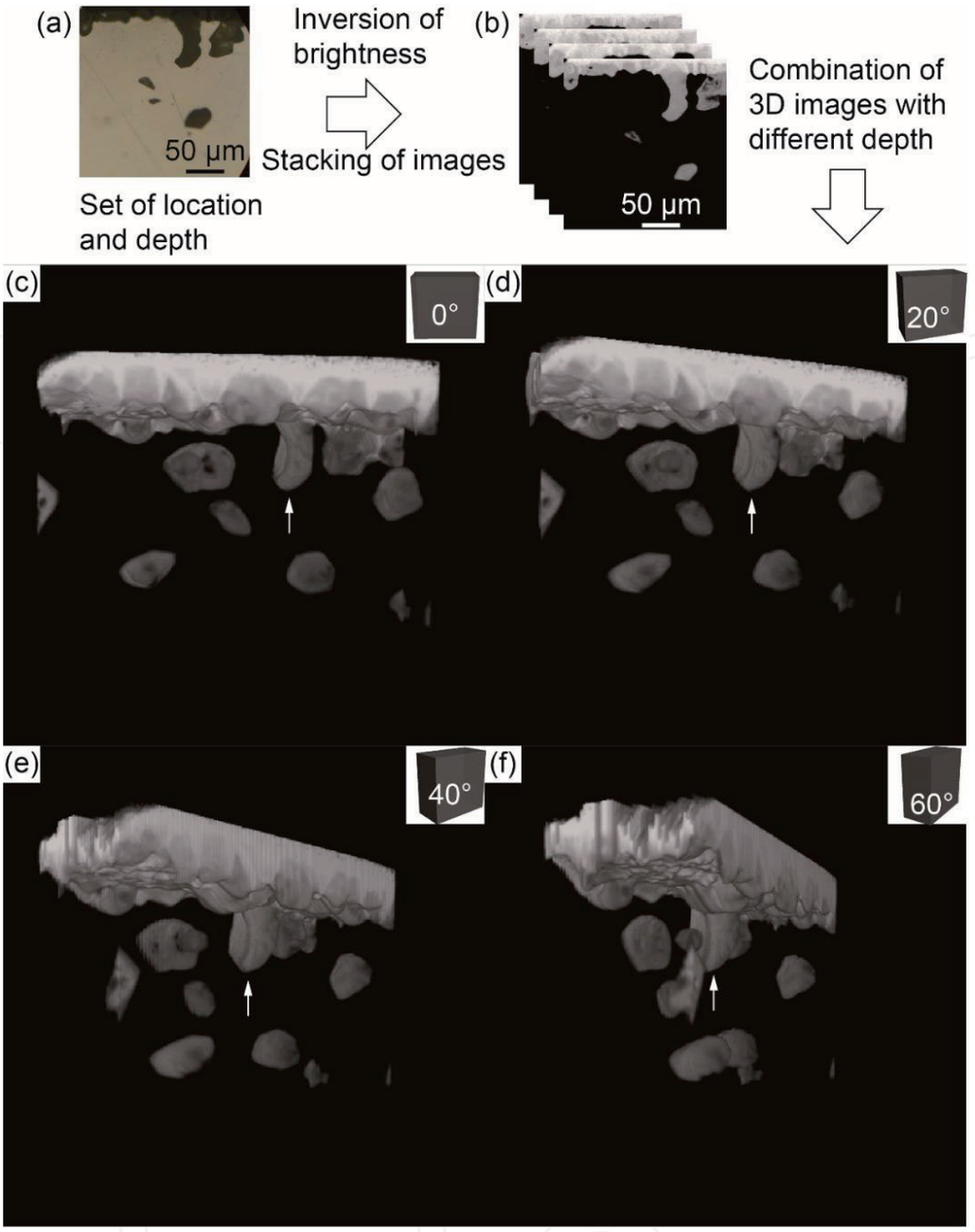

Figure 5.
Three-dimensional microscopic images obtained from optical micrographs of cold rolled and hydrogenated AZ61 for 129.6 ks (a) a sample of optical micrograph, (b) samples of inverted black and white micrographs, and three-dimensional images (c) 0°, (d) 20°, (e) 40°, and (f) 60°.

three-dimensional analysis was conducted at the area shown in **Figure 5**. **Figure 5** taken from cold rolled and hydrogenated AZ61 sample show (a) part of OM micrograph, (b) MgH_2(sur) and MgH_2(int) extracted as ROI area contrast inverted, and construction of three-dimensional image rotated from 0 to 60° ((c) 0°, (d) 20°, (e) 40°, and (f) 60°). From **Figure 5c–f**, the MgH_2(int) was not in contact with hydrogen gas and MgH_2(sur).

Focusing on MgH_2(sur), homogeneous hydride layer does not growth from surface and structure with variations in thickness was spread out in a planar manner with respect to the surface. The white arrow point of MgH_2(sur) was grown abnormally like as heteroepitaxially, however size of the part of MgH_2(sur) was same size with surrounding MgH_2(int), since the part of MgH_2(sur) would be formed by collision between MgH_2(sur) and MgH_2(int) at near surface.

Figure 6 shows an OM micrograph of hydrogenated Mg and a schematic image. Focusing on MgH_2(int), the shape of MgH_2(int) was granular and precipitated on the Mg grain boundary. In addition, two types of MgH_2(int) were observed as growth to two adjacent Mg grains (at pointed two grains) and on only one side of Mg grain. They were indicated in the inset image.

Figure 7 shows the SEM-BSE images of the MgH_2(sur) of hydrogenated Mg, AZ31, AZ61, and AZ91 alloys for 1.8–259.2 ks. Focusing on images of hydrogenated in relatively short time, for example at 1.8 ks, MgH_2(sur) formed with granular and dotted and that was not formed uniformly like a layer at the time when the entire surface was not covered with hydride. With increase of hydrogenation time, the granular hydride, MgH_2(sur), grew in the direction parallel to the surface and formed a rough layer. For images of samples exposed to relatively long hydrogenation time, the thickness of MgH_2(sur) decreased with an increase in Al concentration. **Figure 8** shows the thickness of MgH_2(sur) of Mg, AZ31, AZ61, and AZ91

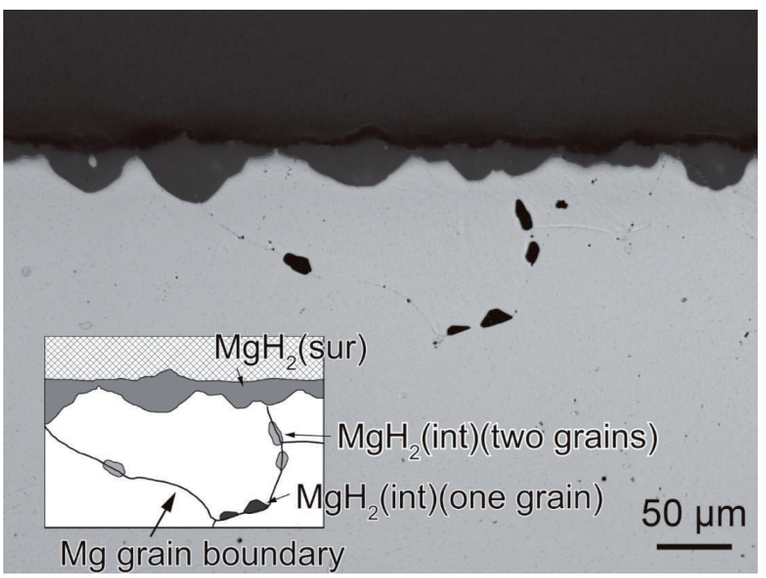

Figure 6.
SEM-BSE image of Mg hydrogenated at 673 K in 3.61 MPa H_2 for 129.6 ks.

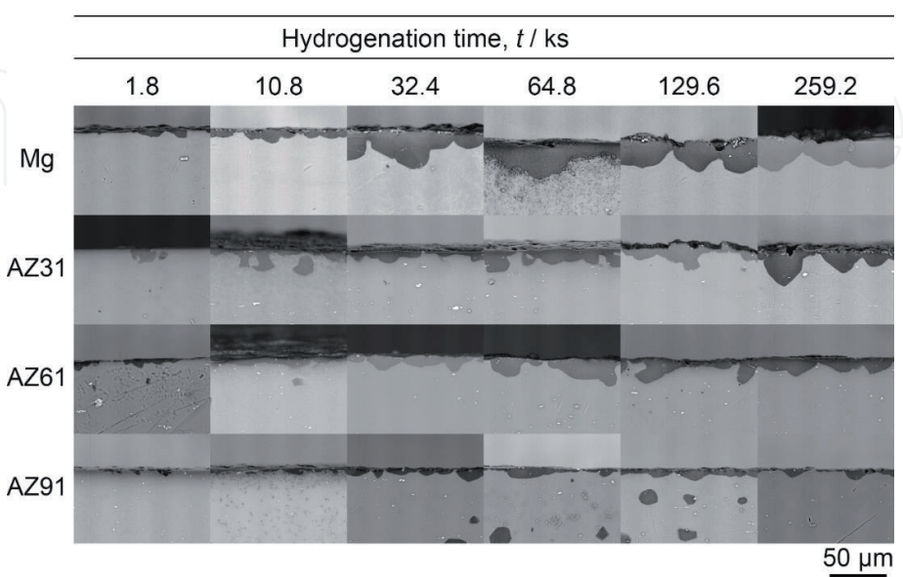

Figure 7.
SEM-BSE images at MgH_2(sur) of Mg, AZ31, AZ61 and AZ91 after hydrogenation at 673 K in 3.61 MPa H_2 for 0–259.2 ks.

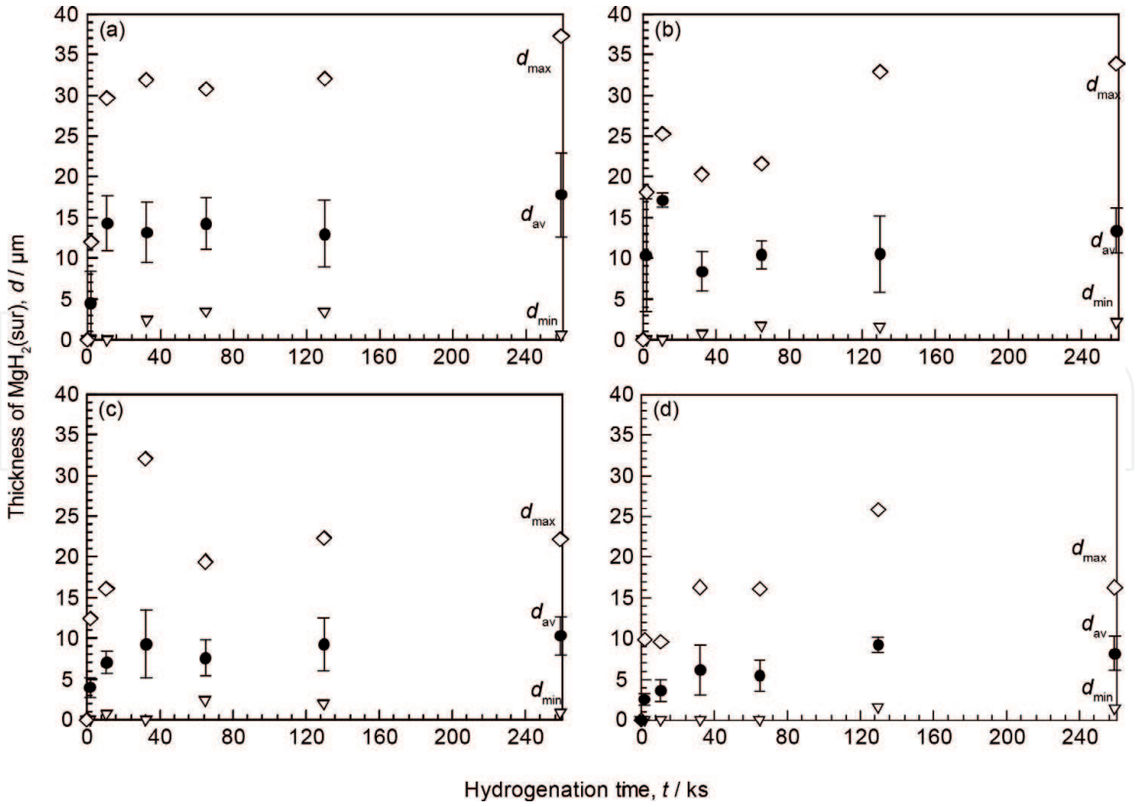

Figure 8.
Relation between thickness of MgH_2(sur) and hydrogenation time of (a) Mg, (b) AZ31, (c) AZ61, and (d) AZ91.

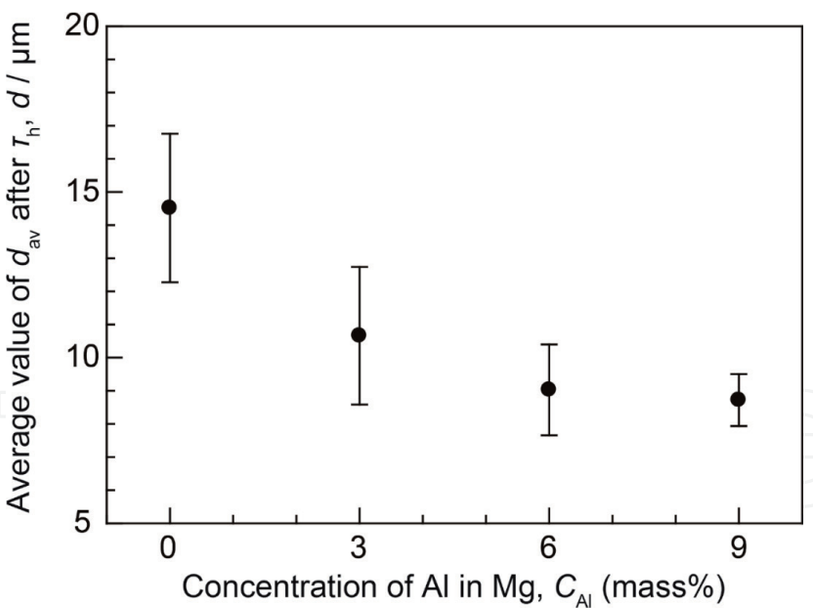

Figure 9.
Relation between average value of d_{av} and concentration of Al in Mg after τ_h.

alloys with hydrogenation time. The white rhombi and the reverse triangles are shown as d_{max} and d_{min}, respectively. The black circles are shown as d_{av} and the vertical lines are expressed as standard deviation. Focusing on d_{min}, d_{min} = 0 means that the surface was not completely covered with MgH_2(sur). Therefore, paying attention to the value of d_{min}, it is possible to estimate the time when entire surface is covered with MgH_2(sur), and the time describes as time of halt (τ_h). τ_h was 32.4 ks for Mg and AZ31, 64.8 ks for AZ61, 129.6 ks for AZ91, and τ_h increased with increasing Al concentration. Next, looking at d_{av}, it was found that d_{av} grew greatly

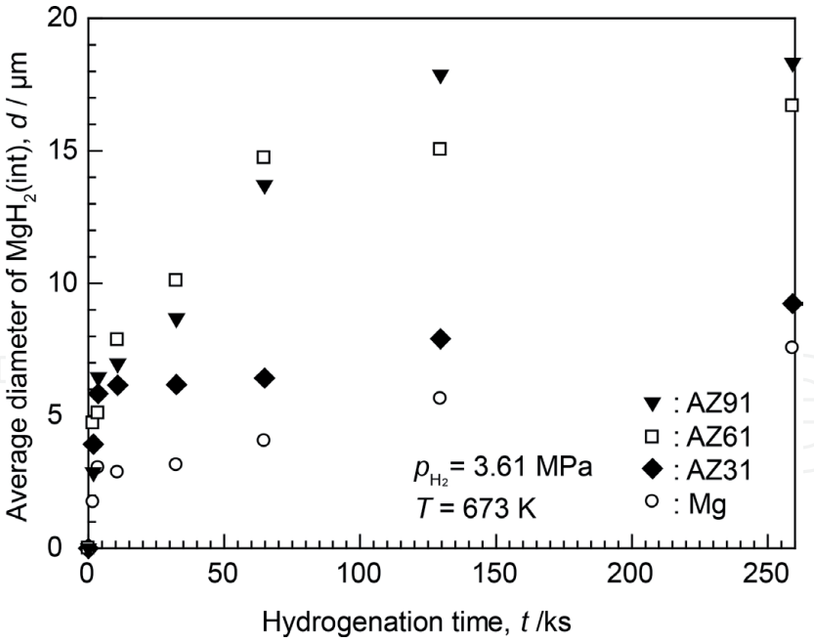

Figure 10.
Relation between average diameter of MgH_2(int) and hydrogenation time of Mg, AZ31, AZ61 and AZ91.

with increasing hydrogenation time before τ_h, whereas the growth rate drastically decreased after the time of τ_h. These results indicate that the growth of MgH_2(sur) halted when sample surface was covered with MgH_2(sur).

To reveal the influence of Al concentration on thickness of MgH_2(sur), the relationship between average of d_{av} after τ_h and Al concentration is shown in **Figure 9**. As shown in **Figure 9**, it was found that the thickness of MgH_2(sur) decreased with the increase of Al concentration, and the decrease ratio is remarkable from 0 to 3 mass% Al than from 6 to 9 mass% Al.

Changes in the growth rate of MgH_2(int) are described as follows. **Figure 10** shows the average particle size of MgH_2(int) of Mg, AZ31, AZ61, and AZ91 alloys with hydrogenation time. As with the changes of MgH_2(sur), the growth rate of MgH_2(int) was high over short time and low on longer hydrogenation time side. The time of infection point was almost correlated with τ_h as 3.6 ks for Mg and AZ31, 64.8 ks for AZ61, 129.6 ks for AZ91. **Figure 10** shows the relationship between the average particle size of MgH_2(int) after τ_h and Al concentration. The average particle size of MgH_2(int) increased with increase of Al concentration, contrary to the change of thickness of MgH_2(sur).

4. Discussion

4.1 Formation of MgH_2 in Mg core

After hydrogenating Mg and AZ alloys, two types of MgH_2 were formed: on the surface, MgH_2(sur) and in the unreacted Mg core, MgH_2(int). MgH_2(int) formed only along Mg grain boundary, and did not form in Mg crystal grain. It is known that the diffusion of H atoms in Mg made the grain boundary a preferential route [20]. Therefore, the reason why MgH_2(int) preferentially formed on grain boundary would be one factor of the fast diffusion of H atoms at Mg grain boundary. In addition, MgH_2 preferentially formed with existence of defect as nanocrystallize Mg showed fast hydrogenation and dehydrogenation [3]. This observation also supports the reason why MgH_2(int) formed on Mg grain boundary.

As shown in **Figure 6**, MgH_2(int) grew for adjacent Mg crystal grain or only on one crystal grain. In addition, some Mg grain boundaries did not form MgH_2(int). Some orientation relationship between Mg and MgH_2 was reported as $(0001)_{Mg}$// $(001)_{MgH2}$, $[-1–120]_{Mg}$//$[001]_{MgH2}$ [21] and $(-2110)_{Mg}$//$(12–1)_{MgH2}$, $[0001]_{Mg}$// $[101]_{MgH2}$ [22]. Because interface energy between new phase and mother phase was low in orientation relationship, solid-solid transformation easily proceeded in orientation relationship with a small lattice mismatch. On the other hand, hydrogenation rate of Mg increased with formation of (0002) crystal texture [23, 24]. Form above results, nucleation and growth of MgH_2(int) would also depend on adjacent Mg crystal orientation. However, influence of Mg crystal texture for MgH_2 formation had other formation of MgO factor [24], and particle shape of MgH_2(int) was ellipsoidal. Therefore, consideration with complex effects for formation of MgH_2(int) should be needed such as orientation relationship, precipitates on Mg grain boundary, interface energy with adjacent Mg grains, and flux of H atom and so on.

4.2 Relationships between particle size of MgH_2(int) and Al concentration

Before τ_h, MgH_2(sur) formed in granular form and spread and the growth rate of average thickness was larger than that after τ_h. After τ_h, the growth of MgH_2(sur) apparently halted. These growth rate change was same in MgH_2(int). These results be attributed to extremely low diffusion rate of H in MgH_2 when compared to that in Mg [12, 13]. When the whole surface was covered with MgH_2(sur), the supply rate of H to unreacted internal metallic Mg or AZ significantly decreased, halting the growth of MgH_2(sur) and MgH_2(int).

Some studies have reported that the amount of MgH_2 formed depends on Gibbs free energy ($\Delta_r G$) of MgH_2 from Mg and H_2 gas [16, 25, 26]. The microstructure of MgH_2(sur) at initial state was formed as granular and scattered. Concerning this result, the nucleation rate of MgH_2(sur) was low and the nucleation rate would depend on absolute value of $\Delta_r G$. Applying low value of $\Delta_r G$, growth of MgH_2(int) proceeded because nucleation rate of MgH_2(sur) was low and τ_h is shift to longer time. However, when high value of $\Delta_r G$ was applied, the nucleation rate of MgH_2(sur) increased and immediately the surface covered with thin MgH_2(sur) rapidly and the particle size of MgH_2(int) was explained to be small size.

The average particle size of MgH_2(int) increased with increasing Al concentration. As shown in **Figure 10**, the growth rate of MgH_2(int) decreased when the surface was covered with MgH_2(sur). The thickness of MgH_2(sur) decreased with increasing Al concentration. From these results, the reasons why the particle size of MgH_2(int) decreased with increasing Al concentration would be shifting of long time τ_h and small diffusion distance of H in MgH_2 at high Al content. Therefore, the amount of supplying H increased and large size of MgH_2(int) formed with increasing Al concentration.

5. Conclusion

In this study, focusing on the formation of MgH_2 in the Mg core, the effects of Al concentration in Mg for microstructure of hydrogenated Mg and Mg-Al-Zn alloys were investigated. MgH_2(int) formed at Mg grain boundary and the growth rate of MgH_2(int) was investigated including plastic deformed condition. From three-dimensional analysis, it was found that the MgH_2(int) was surrounded by metallic Mg or Mg-Al-Zn alloys and they had not interfaced with H_2 gas and MgH_2 on the surface area(sur). The time when the surface covered with MgH_2(sur) was described as time of halt, τ_h. Comparing growth rate of MgH_2(sur) and MgH_2(int)

before and after τ_h, the growth rate of both MgH_2 were higher before τ_h than after τ_h. The growth of MgH_2(sur) and MgH_2(int) were observed to stop after τ_h because H supply route change from in Mg to MgH_2. After τ_h, the thickness of MgH_2(sur) decreased and particle size of MgH_2(int) increased with increasing Al concentration. This result could be explained by increase of supplied H amount to MgH_2(int) due to the shifting τ_h to longer time and small diffusion distance of MgH_2(sur) which had low value of diffusion coefficient.

Findings from this research point out in following:

- Hydrogenated Mg plate formed MgH_2 on surface(sur) and in internal area(int).
- The thickness of MgH_2(sur) decreased with increase of Al concentrations in Mg.
- The particle size of MgH_2(int) increased with increase of Al concentrations in Mg.

Acknowledgements

This is a product of research which was financially supported by JSPS KAKENHI Grant Number 19K15278, and the Environment Research and Technology Development Fund (2RF-1801) of the Environmental Restoration and Conservation Agency of Japan.

Author details

Ryota Kondo* and Takeshita T. Hiroyuki
Department of Chemistry and Materials Engineering, Faculty of Chemistry, Materials and Bioengineering, Kansai University Suita, Osaka, Japan

*Address all correspondence to: rkondo@kansai-u.ac.jp

References

[1] Jehan M, Fruchart D. McPhy-Energy's proposal for solid state hydrogen storage materials and systems. Journal of Alloys and Compounds. 2013;**580**:S343-S348

[2] Schlapbach L, Züttel A. Hydrogen-storage materials for mobile applications. Nature. 2001;**414**:353-358

[3] Zaluska A, Zaluski L, Ström-Olsen JO. Nanocrystalline magnesium for hydrogen storage. Journal of Alloys and Compounds. 1999;**288**:217-225

[4] Varin RA, Czujko T, Chiu C, Wronski Z. Particle size effects on the desorption properties of nanostructured magnesium dihydride (MgH2) synthesized by controlled reactive mechanical milling (CRMM). Journal of Alloys and Compounds. 2006;**424**:356-364

[5] Oelerich W, Klassen T, Bormann R. Hydrogen sorption of nanocrystalline Mg at reduced temperatures by metal-oxide catalysts. Advanced Engineering Materials. 2001;**3**:487-490

[6] Barkhordarian G, Klassen T, Bormann R. Fast hydrogen sorption kinetics of nanocrystalline Mg using Nb2O5 as catalyst. Scripta Materialia. 2003;**49**:213-217

[7] Shibata K, Tanaka K, Kurumatani K, Nishida Y, Kondo R, Takeshita HT. Formation of MgCu2 from MgH2 and Cu in pressurized hydrogen atmosphere. Materials Transactions. 2015;**56**:785-789

[8] Tanaka K, Takeshita HT, Kurumatani K, Miyamura H, Kikuchi S. The effect of initial structures of Mg/Cu super-laminates on hydrogen absorption/desorption properties. Journal of Alloys and Compounds. 2013;**580**:S222-S225

[9] Tanaka K, Takeshita HT, Shin H, Kurumatani K, Kiyobayashi T, Takeichi N, et al. Micro/nano-structural transition and hydrogen absorption mechanism in Mg/Cu super-laminate composites. Materials Transactions. 2014;**55**:1122-1128

[10] Tanaka K, Shibata K, Kurumatani K, Ikeuchi S, Kikuchi S, Kondo R, et al. Formation mechanism of micro/nano-structures through competitive reactions in Mg/Cu super-laminate composites during initial hydrogenation. Journal of Alloys and Compounds. 2015;**645**:S72-S75

[11] Noritake T, Towata S, Aoki M, Seno Y, Hirose Y, Nishibori E, et al. Charge density measurement in MgH2 by synchrotron X-ray diffraction. Journal of Alloys and Compounds. 2003;**356-357**:84-86

[12] Uchida HT, Wagner S, Hamm M, Kürschner J, Kirchheim R, Hjörvarsson B, et al. Absorption kinetics and hydride formation in magnesium films: Effect of driving force revisited. Acta Materialia. 2015;**85**:279-289

[13] Yang B, He Y-P, Zhao Y-P. Hydrogenation of magnesium nanoblades: The effect of concentration dependent hydrogen diffusion. Applied Physics Letters. 2011;**98**:081905

[14] Shriniwasan S, Tien H-Y, Tanniru M, Ebrahimi F, Tatiparti SSV. Transition from interfacial to diffusional growth during hydrogenation of Mg. Materials Letters. 2015;**161**:271-274

[15] Friedlmeier G, Groll M. Experimental analysis and modelling of the hydriding kinetics of Ni-doped and pure Mg. Journal of Alloys and Compounds. 1997;**253-254**:550-555

[16] Tien H-Y, Tanniru M, Wu C-Y, Ebrahimi F. Effect of hydride nucleation rate on the hydrogen capacity of Mg. International Journal of Hydrogen Energy. 2009;**34**:6343-6349

[17] Ueda TT, Tsukahara M, Kamiya Y, Kikuchi S. Preparation and hydrogen storage properties of Mg–Ni–Mg2Ni laminate composites. Journal of Alloys and Compounds. 2005;**386**:253-257

[18] Abràmoff MD, Magalhães PJ, Ram SJ. Image processing with ImageJ. Biophotonics International. 2004;**11**:36-42

[19] Schneider CA, Rasband WS, Eliceiri KW. NIH Image to ImageJ: 25 years of image analysis. Nature Methods. 2012;**9**:671-675

[20] Uchida HT, Kirchheim R, Pundt A. Influence of hydrogen loading conditions on the blocking effect of nanocrystalline Mg films. Scripta Materialia. 2011;**64**:935-937

[21] Schober T. The magnesium-hydrogen system: Transmission electron microscopy. Metallurgical Transactions A. 1981;**12**:951-957

[22] Nogita K, Tran XQ, Yamamoto T, Tanaka E, McDonald SD, Gourlay CM, et al. Evidence of the hydrogen release mechanism in bulk MgH2. Scientific Reports. 2015;**5**:8450

[23] Jorge AM Jr, Prokofiev E, Ferreira de Lima G, Rauch E, Veron M, Botta WJ, et al. An investigation of hydrogen storage in a magnesium-based alloy processed by equal-channel angular pressing. International Journal of Hydrogen Energy. 2013;**38**:8306-8312

[24] Jorge AM, de Lima GF, Triques MRM, Botta WJ, Kiminami CS, Nogueira RP, et al. Correlation between hydrogen storage properties and textures induced in magnesium through ECAP and cold rolling. International Journal of Hydrogen Energy. 2014;**39**:3810-3821

[25] Mooij L, Dam B. Nucleation and growth mechanisms of nano magnesium hydride from the hydrogen sorption kinetics. Physical Chemistry Chemical Physics. 2013;**15**:11501-11510

[26] Mooij L, Dam B. Hysteresis and the role of nucleation and growth in the hydrogenation of Mg nanolayers. Physical Chemistry Chemical Physics. 2013;**15**:2782-2792